© 2018. Published by The Company of Biologists Ltd | Journal of Experimental Biology (2018) 221, jeb186791. doi:10.1242/jeb.186791

RESEARCH ARTICLE

Alligator mississippiensis sternal and shoulder girdle mobility increase stride length during high walks

David B. Baier[1,*], Brigid M. Garrity[2], Sabine Moritz[3] and Ryan M. Carney[4]

ABSTRACT

Crocodilians have played a significant role in evolutionary studies of archosaurs. Given that several major shifts in forelimb function occur within Archosauria, forelimb morphologies of living crocodilians are of particular importance in assessing locomotor evolutionary scenarios. A previous X-ray investigation of walking alligators revealed substantial movement of the shoulder girdle, but as the sternal cartilages do not show up in X-ray, the source of the mobility could not be conclusively determined. Scapulocoracoid movement was interpreted to indicate independent sliding of each coracoid at the sternocoracoid joint; however, rotations of the sternum could also produce similar displacement of the scapulocoracoids. Here, we present new data employing marker-based XROMM (X-ray reconstruction of moving morphology), wherein simultaneous biplanar X-ray video and surgically implanted radio-opaque markers permit precise measurement of the vertebral axis, sternum and coracoid in walking alligators. We found that movements of the sternum and sternocoracoid joint both contribute to shoulder girdle mobility and stride length, and that the sternocoracoid contribution was less than previously estimated. On average, the joint contributions to stride length (measured with reference to a point on the distal radius, thus excluding wrist motion) are as follows: thoracic vertebral rotation 6.2±3.7%, sternal rotation 11.1±2.5%, sternocoracoid joint 10.1±5.2%, glenohumeral joint 40.1±7.8% and elbow 31.1±4.2%. To our knowledge, this is the first evidence of sternal movement relative to the vertebral column (presumably via rib joints) contributing to stride length in tetrapods.

KEY WORDS: Crocodilians, Joint, Bone, Kinematics, Locomotion, Forelimb

INTRODUCTION

Extant crocodilians have been central to interpreting locomotor evolution of Archosauria (Gatesy, 1991; Hutchinson, 2006; Reilly and Elias, 1998), because of their unique locomotor capacities and relatively basal phylogenetic position. Several major evolutionary changes in primary locomotor mode occur on the line to and within archosaurs: the origin of parasagittal gaits (Padian et al., 2010; Parrish, 1987), two of the three origins of vertebrate flight (pterosaurs and birds), the origin of bipedalism in dinosaurs (Persons and Currie, 2017) and possibly pterosaurs (Padian, 2008), and multiple secondary returns to quadrupedalism (Maidment et al., 2014; VanBuren and Bonnan, 2013). All of these transitions involve changes in the types of external forces experienced by the forelimb which, in turn, affect the kinematics and kinetics of the limb joints. Hence, understanding limb joint function during crocodilian locomotion may help us to interpret evolutionary scenarios within Archosauria.

Many aspects of crocodilian forelimb functional morphology are becoming more clear: detailed muscle morphology (Allen et al., 2014; Meers, 2003; Otero et al., 2017), joint ranges of motion (Hutson and Hutson, 2012, 2013, 2014), skeletal variation (Chamero et al., 2013; Iijima et al., 2018) and joint kinematics (Baier and Gatesy, 2013). One major finding in the study of Baier and Gatesy (2013) was a surprising degree of shoulder girdle mobility, which contributed substantially to the overall stride length. This could represent an intriguing convergence with therian mammals, whose loss of the primary articulation between shoulder girdle and sternum allowed the scapula to act as an additional limb segment, resulting in increased stride length (Eaton, 1944). This mobility is further enhanced in several eutherian mammalian groups by loss of the clavicle, which connects the scapula to the sternum. Clavicular loss also occurred on the line to Crocodylomorpha and could also be related to shoulder girdle mobility.

However, the anatomy of the alligator shoulder girdle makes it particularly challenging to study, even in X-ray video. The shoulder girdle is composed of a dorsal scapula and ventral coracoid, both of which contribute to the glenoid articulation with the humeral head. The coracoid forms a tongue-and-groove joint (sternocoracoid joint) ventrally with the sternum (Fig. 1). The cartilaginous sternum, which contains a central, thin bony interclavicle, was not visible in dorsal X-ray views (Baier and Gatesy, 2013). Thus, displacement of the scapulocoracoid was measured relative to the vertebral column and interpreted to be sternocoracoid joint movement. However, if the sternum/interclavicle unit moves relative to the vertebral column (via rib cage deformations), displacement of the scapulocoracoid could occur without any movement of the sternocoracoid joint, as was noted by Baier and Gatesy (2013).

In this study, we applied marker-based XROMM (Brainerd et al., 2010; http://xromm.org) to measure the movement of the sternum/interclavicle unit independently from that of the scapulocoracoid in alligators performing high-walks on a treadmill. This allowed us to test whether observed shoulder girdle displacement relative to the vertebral column is derived from (1) sternocoracoid joint motion, (2) rotations of the sternum/interclavicle unit or (3) some combination of 1 and 2.

MATERIALS AND METHODS

Animals

Two alligators (Ag1, Ag2), *Alligator mississippiensis* (Daudin 1802), were surgically implanted with markers specifically for use in this study. Data from an additional two alligators (Ag3, Ag4)

[1]Providence College, Department of Biology, Providence, RI 02918, USA. [2]Boston University, School of Graduate Medical Science and School of Public Health, Boston, MA 02118, USA. [3]Brown University, Ecology and Evolutionary Biology, Providence, RI 02912, USA. [4]University of South Florida, Department of Integrative Biology, Tampa, FL 33620, USA.

*Author for correspondence (dbaier@providence.edu)

D.B.B., 0000-0003-2139-6609

Received 14 June 2018; Accepted 20 September 2018

Journal of Experimental Biology (2018) 221, jeb186791. doi:10.1242/jeb.186791

List of abbreviations

ACS	anatomical coordinate system
EST	end of stance
GHJ	glenohumeral joint
IMD	inter-marker distance
JCS	joint coordinate system
SCJ	sternocoracoid joint
SST	start of stance
SSW	start of swing
XROMM	X-ray reconstruction of moving morphology

were shared from XMAPortal: Alligator Breathing project (Brocklehurst et al., 2017) and further analyzed in this study. The two fully marked alligators (Table 1) were housed and cared for in the animal care facility at Brown University in accordance with approved protocol procedures. Radio-opaque markers were surgically implanted into skeletal elements. Following recovery for 1–2 weeks, synchronized, biplanar X-ray videos of the alligators walking on a treadmill were captured. At the end of the experiment, animals were euthanized by overdose via intravenous injection of 1 ml of 200 mg kg^{-1} pentobarbital (Beuthanasia-D®, Merck Animal Health/Intervet Inc., Madison, NJ, USA) and frozen for later computed tomography scans and dissections. The alligators from the Alligator Breathing project had only the vertebral markers and sternal markers implanted. All X-ray and CT data are stored in the X-ray Motion Analysis Portal (xmaportal.org).

Marker implantation and surgery

Alligators were initially sedated with an intramuscular injection of butorphanol and then induced and anesthetized with isoflurane. Five to eight tantalum beads (either 0.8 or 1.0 mm) were implanted into the thoracic scutes, spanning 4–5 thoracic vertebrae in the region of the shoulder girdle (T2–T6: Ag1 and Ag2, T6–T9: Ag3 and Ag4); 0.8 mm beads were implanted into the paired cartilaginous sterna/interclavicle complex (3–4 beads), coracoid (3), scapula (3) and humerus (3–4). Additional markers were implanted into more distal elements, but only the distal phalanx markers for digits 2, 3 or 4 (depending on which was most clearly visible) were used to measure tread velocity, whereas a distal radius marker was used to measure stride length and phasing.

X-ray video

Biplanar X-ray video (72–75 kV, 200 mA, 2 ms pulsed intervals) was collected in the W. M. Keck Foundation XROMM facility (for hardware details, see http://www.xromm.org/hardware). Photron v9 cameras captured dorsoventral and lateral views at 100 frames s^{-1} with shutter speeds from 1/600 to 1/700.

Computed tomography (CT) and bone model mesh reconstruction

Following euthanasia and freezing, the carcasses were CT scanned. Three alligators were scanned at Rhode Island Hospital (technique: 80 kVp, 80 mA, slice thickness 0.625 mm). One alligator was scanned at Brown University using a Fidex (Animage) scanner

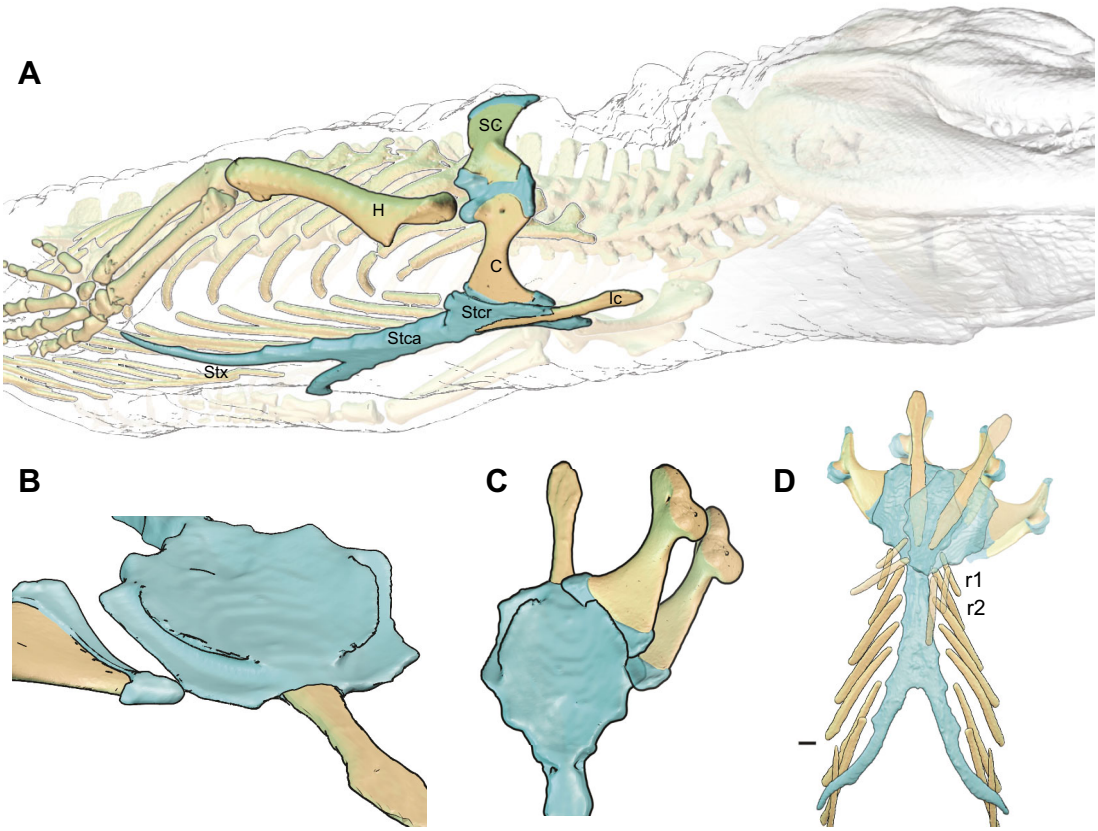

Fig. 1. Alligator shoulder girdle anatomy. (A) Lateroventral view of the shoulder girdle and right forelimb of an American alligator (*Alligator mississippiensis*). (B) Cranio-dorsal view of the dorsal aspect of the coracosternal joint disarticulated to show the tongue (ventral coracoid) and groove (on the antero-lateral aspect of the sternal cartilage). (C) Dorsal view of the coracosternal joint showing the approximate cranial and caudal limits of sliding along the groove, based on dissections with all muscles removed. (D) Ventral view of the sternum showing the primary bending zone between the prosternum and mesosternum. Scale bar: 10 mm. C, coracoid; H, humerus; Ic, interclavicle; r, rib; Stca, caudal sternum (mesosternum); Stcr, cranial sternum (prosternum); Stx, xiphoid processes.

Journal of Experimental Biology (2018) 221, jeb186791. doi:10.1242/jeb.186791

Table 1. Specimen summary

Alligator	Mass (kg)	Humeral length (mm)	SCJ length (mm)	XMA portal name	XMA portal study
Ag1	3.4	68.6	19.9	Ag2r2	Alligator forelimb
Ag2	4.0	71.4	20.0	Ag6r2	Alligator forelimb
Ag3	3.0	65.9	17.4	Ag1L5	Alligator lung ventilation
Ag4	2.9	64.7	19.2	Ag5L5	Alligator lung ventilation

SCJ, sternocoracoid joint.

(technique: 110 kVp, 31 mA, slice thickness 0.3925 mm). 3D polygonal bones and marker meshes were extracted (OsiriX) and refined (Geomagic Studio 12) to create manifold shell meshes and evenly spaced vertices. Mesh bone models were then imported into Maya 2016 (Autodesk), where the centroids of marker meshes were calculated using XROMM Maya tools (https://bitbucket.org/xromm/xromm_mayatools).

Coordinate systems

Joint coordinate systems (JCSs) for (1) a thoracic vertebral segment, (2) the sternum+interclavicle, (3) the sternocoracoid joint and (4) the glenohumeral joint were created by defining proximal and distal anatomical coordinate systems (ACSs) for each joint. Joint motion is measured as the position and orientation of the distal ACS relative to the proximal ACS. The basic pattern follows Baier and Gatesy (2013), but here we incorporated specific procedures for defining each ACS and JCS. We first calculated principal (inertial) axes for each bone mesh (Crisco and McGovern, 1998) and then used customized algorithms in Matlab and Maya to identify key skeletal landmarks that could be used to place and orient the axes.

Thoracic vertebral coordinate system

Five thoracic vertebrae (T2–T6 or T4–T8) were treated as a rigid body for the purpose of measuring vertebral movement relative to the experimental coordinate system. X+ pointed caudally, Y+ pointed to the right and Z+ pointed dorsally. Positive roll (about the *X*-axis) was towards the left limb. Positive pitch (about the *Y*-axis) was nose up. Positive yaw (about the *Z*-axis) was to the left. The proximal ACS for the thoracic segment is the treadmill coordinate space. Movements of the vertebral column were initially measured in calibration coordinate space and then transformed into treadmill coordinate space. Treadmill coordinate space was determined by reconstructing the X-ray camera setup in Maya (Autodesk), creating a polygonal mesh model of the tread, and aligning the tread model to the two X-ray views.

Interclavicle/sternal JCS

The cartilaginous sternum, which bears the articular surface for the sternocoracoid joint, could not be clearly segmented from CT scans of intact alligators. Thus, cartilage models were reconstructed by isolating and cleaning the shoulder girdle elements of a non-experimental specimen, leaving cartilages intact. This specimen was CT-scanned and segmented both for bone and for cartilage (possible because of the contrast between air and cartilage). The interclavicle was then scaled and fitted to each experimental animal using a custom Maya MEL script. The same transforms were applied to the model of the cartilaginous sternum.

The proximal ACS, which moves with the thoracic vertebral segment, had the same orientation and medio-lateral (*Y*) position as the vertebral ACS but was at the cranio-caudal (*X*) and dorso-ventral (*Z*) position of the inertial axes of the reconstructed sternal cartilage (sans xiphoid processes). The distal ACS was defined by the inertial axes of the reconstructed sternal cartilage excluding the xiphoid processes. X+ pointed caudally, Y+ pointed to the right and Z+ pointed dorsally.

Sternocoracoid JCS

The tongue and groove sternocoracoid joints (SCJs) constitute articulations between the ventral ends of the coracoids (tongues) and the sternal grooves on the cranio-lateral surface of the sternum. The cartilaginous sternum reconstruction was needed to consistently find the location of the proximal ACS. A mesh model of the sternal groove was made in Geomagic by deleting all faces of the sternal cartilage model except those forming the inside of the joint surface. The mesh was then closed by bridging the open edge of the joint. The inertial axes of the joint 'cast' mesh model provided the orientation and the center point of the proximal ACS. X+ pointed caudo-medially, perpendicular to the long axis of the obliquely oriented sternal groove. Y+ pointed caudo-laterally, parallel with the long axis of the groove. Z+ pointed cranio-dorsally and matched the *YZ*-plane orientation of the sternal ACS.

The distal ACS of the 'tongue' side of the joint was found by reconstructing the ventral coracoid articular cartilage, which entailed scaling and fitting the dissection specimen coracoid to the experimental specimen (as was done to reconstruct the sternal cartilage). The distal ACS was placed at the center of the cartilage model volume along the midpoint of the long axis. X+ pointed caudo-medially, perpendicular to the long axis of the tongue cartilage. Y+ pointed caudo-laterally, parallel with the long axis of the tongue cartilage. Z+ pointed dorsally and paralleled the long axis of the scapulocoracoid.

Rotations about the *Z*-axis are termed protraction (+) and retraction (−). Rotations about the *Y*-axis are termed adduction (+) and abduction (−). Rotations about the *X*-axis are termed pronation (+) and supination (−).

Glenohumeral JCS

The proximal ACS of the glenohumeral joint (GHJ) was positioned by averaging of vertices along the rim of the coracoid and scapular facets. Orientation was set to match sternal ACS after the sternum and SCJs were positioned and oriented in their zero reference pose.

The distal ACS of the GHJ was positioned at the center of the humeral head with the *X*-axis matching the long axis of the entire bone (least axis of inertia; X+ pointed medially) and the *Y*-axis paralleling the distal condyles (maximum inertial axis of the distal half of the bone; Y+ pointed caudally), which resulted in the *Z*-axis being perpendicular to the condyles (Z+ pointed dorsally).

Kinematics

XMALab (https://bitbucket.org/xromm/xmalab) was used to track marker positions during walking. Rigid body transformation matrices obtained from XMALab were used to animate bone models in Maya 2016 (Autodesk, Inc.) using XROMM Maya tools (https://bitbucket.org/xromm/xromm_mayatools). Kinematic measurements were then calculated from the JCSs described above. Stance and swing phases for strides were visually assessed. In lateral

Journal of Experimental Biology (2018) 221, jeb186791. doi:10.1242/jeb.186791

view, the surface of the tread depressed slightly at the start of stance (SST). The end of stance and start of swing (SSW) was taken to be the moment when the all fingers had lifted from the tread. The end of the stride (EST) was the following foot contact.

Average tread velocity for each stride was calculated as change of position of a single finger marker from a frame near the beginning of stance to a frame near the end of stance, divided by change in time. Duty factor or percentage of time in stance phase was calculated as stance frames divided by total stride frames.

Tread velocity and duty factor were calculated using the raw, non-scaled timing. For all other kinematic measurements, stance and swing phases were time-scaled to 100 time steps using a custom Maya script. The average duty factor of all strides (72%) was used to scale all strides as follows: SST to SSW minus one was scaled from 0 to 71% of the stride, and SSW to EST was scaled from 72% to 100%. As finger markers were at times obscured by the tread, stride length was measured using a marker on the radius (thus excluding the movements of the wrist and finger joints). Because the distal radius was often out of view at the beginning of stance in the rotoscoped alligators, the radius was rotoscoped to provide a distal wrist position for analysis of stride loops.

Statistics

Basic statistics were calculated in Matlab. Means and standard deviations reported in the tables and text were calculated for each individual and were also pooled for all individuals. One-way ANOVA was used to test for significant differences among individuals. If no individuals differed significantly, only the pooled data for all individuals were reported, but significant differences found are described in the text.

Graphs were plotted by calculating a mean and standard deviation for each time step for each degree of freedom for each individual across all strides for that individual, and for all individuals by averaging across all strides for all individuals.

Note that statistics in the tables and text are calculated differently from data in the graphs. Text and table data are averages per stride while graphs are per time step averages. As peak values may not occur at exactly the same time step across all strides, the averaged graph curves may appear to have slightly different peaks and peak event timings from those expected based on the information in the text and tables.

Validation

Kinematic measurements assume that skeletal elements are not bending or deforming. If structures are truly rigid, inter-marker distance (IMD) standard deviations between markers on the same rigid element should be low. To establish expected IMD standard deviations, a single frozen alligator with markers implanted in the forelimb and girdle elements was waved through the X-ray volume at a frequency approximating strides. Markers were tracked in XMALab for 986 frames at 100 frames s^{-1}. Rigid body IMD standard deviations positively correlate with IMD of markers tracked in XMALab (Knorlein et al., 2016) as was the case in this study (P<0.0001). The linear regression equation y=0.00098x+0.0025 was used to predict standard deviation for a given IMD for all markers in the experimental animals. If the actual calculated IMD standard deviation for the experimental animal was less than the maximum residual of predicted standard deviation, it was considered to be within the expected range for a pair of markers on the rigid body.

Precision thresholds were established by measuring joint motion from a frozen alligator waved through the X-ray volume at a cadence approximating the stride frequency of the experimental animals (Brainerd et al., 2016; Menegaz et al., 2015). As no joint motion should occur in the frozen specimen, measured variation represents noise. For each kinematic degree of freedom in the experimental animals, the mean plus and minus the standard deviation from the frozen alligator was used to set the threshold for measurable motion.

RESULTS

Anatomy

The alligator sternum is composed of a prosternum, mesosternum and xiphisternum (Kälin, 1929). The prosternum is a diamond-shaped, cartilaginous cranial portion (bearing a midline, cranially projecting bony interclavicle, and articular surfaces for the coracoids and the first two rib pairs). The mesosternum is a narrow, caudal body (bearing articular surfaces for ribs three to six). The xiphisternum consists of two caudal processes, to which the remaining ribs attach (Fig. 1A,D). The junction between the prosternum and mesosternum is highly mobile and permits the prosternum and the interclavicle to move as a unit relative to the vertebral column, the caudal thorax and abdomen. With ribs cut and muscles removed, this bending zone permits approximately 30 deg of yaw in each direction. Flexibility of the mesosternum can also contribute to yaw of the prosternum (Fig. 1D).

The tongue-shaped cartilages on the ventral ends of the coracoids articulate with paired antero-laterally facing grooves on either side of the sternum (Fig. 1B). The SCJ primarily permits sliding of the tongue of the coracoid articular cartilage along the long axis of the sternal groove when manipulated in dissected preparations (Fig. 1C). Sliding combined with protraction/retraction displaces the glenoid craniocaudally. Tension in the connective tissues extending from the sternum and interclavicle to the coracoid limits caudal sliding, and connective tissues extending from the caudal aspect of the sternal groove to the coracoid limit cranial sliding. The cartilages are somewhat flexible and can deform to permit a small degree of abduction/adduction and pronation/supination.

Kinematics

Mean duty factor was 0.73±0.06 (Table 2). Raw stride length, measured as the change in position of the distal radius in the direction of the treadmill, averaged 0.17±0.03 m. Stride length in the vertebral reference frame was 0.18±0.01 m. Mean stride frequency was 0.48±0.07 Hz. Average velocity was 0.15±0.04 m s^{-1} (36 strides) but one individual (Ag2) walked more slowly than the other three (one-way ANOVA; P<0.001). Mean tread velocity for the three non-differing alligators was 0.17±0.03 m s^{-1} (27 strides), compared with 0.10±0.02 m s^{-1} (9 strides) for Ag2 (Table 2). For the following sections on joint kinematics, timing of events is often of interest with reference to both the stride and phase of stride (stance/swing). Thus, we report results as both a percentage of stride and a percentage of stance phase or swing phase where appropriate.

Table 2. General kinematic data summary

Alligator	Tread velocity per stride (m s^{-1})	Duty factor	Stride frequency (Hz)	Stride length (m)
Ag1 (N=9)	0.17±0.02	0.69±0.02	0.50±0.04	0.16±0.01
Ag2 (N=9)	**0.10±0.02**	0.74±0.03	0.43±0.08	0.16±0.02
Ag3 (N=9)	0.16±0.04	0.76±0.07	0.50±0.06	0.19±0.03
Ag4 (N=9)	0.17±0.03	0.74±0.06	0.47±0.07	0.17±0.02
All (N=36)	0.15±0.04	0.73±0.05	0.48±0.07	0.17±0.03

Data are means±s.d. Bold indicates a significant difference from data for the other specimens (P<0.001).

Journal of Experimental Biology (2018) 221, jeb186791. doi:10.1242/jeb.186791

Movements of the shoulder region vertebral segment relative to the treadmill

Vertebrae T2–T6 in the fully marked alligators (Ag1, Ag2) and T6–T9 in the partially rotoscoped alligators (Ag3, Ag4; see Materials and Methods) were treated as a single rigid body, indicating the movements of the spine in the region of the shoulder girdle relative to the treadmill coordinate space (Fig. 2, Table 3).

The vertebral segment yawed 16.5±3.2 deg on average (Fig. 2, blue). The thorax was yawing towards the left at the beginning of right forelimb stance, reached peak left yaw (8.3±2.6 deg) at 11% of stride (15±7% of stance) and then began yawing towards the stance limb, reaching peak right yaw (−8.2±1.5 deg) at 60% of stride (84±10% of stance). During the remainder of swing phase, the vertebral segments yawed left.

Vertebral pitch (Fig. 2, green) and roll (Fig. 2, red) motions were subtler, with ranges per stride of 5.5±2.1 deg and 7.6±2.7 deg, respectively. The mean pitch angle was −11.8±4.2 deg (nose down). Peak timing events could only be clearly discerned in Ag1. In Ag1, pitch increased during stance and decreased during swing, reaching a peak at 54% of stride (74±3% of stance). Roll increased (away from the stance limb) for Ag1 during stance and reached peak at 52% of stride (72±9% of stance).

Movements of the sternum/interclavicle unit relative to the vertebral segments

Sternal yaw, pitch, roll and lateral translation exceeded noise thresholds (Fig. 3, Table 3). Both cranio-caudal translation and vertical translation produced patterned curves that were consistent across strides, but fell below the noise threshold, with mean ranges per stride of 0.36±0.16 mm and 0.24±0.09 mm, respectively.

The sternum yawed 25.8±6.0 deg over the course of a stride. The sternum was yawing left at the beginning of right limb stance, reaching peak left yaw at 5% of stride (6±4% of stance), and then yawed towards the stance limb, reaching peak right yaw at 49% of stride (68±5% of stance) (Fig. 3A–C, blue). Pitch range was 5.8±1.9 deg, with a mean pitch angle of 17.6±3.6 deg relative to the vertebral segments (Fig. 3A,B,D, green) where positive pitch is nose up. Roll range was 23.5±5.2 deg. At the beginning of right limb stance, the sternum was rolling left, reaching a peak of 11.7±4.3 deg at 19% of stride (26±5% of stance). Roll towards the stance limb ensued through most of stance, reaching a peak of −11.8±6.5 deg at 65% of stride (90±12% of stance) (Fig. 3A,B,D, red). The sternum was laterally displaced to the left at the beginning of right limb stance, then translated 11.9±0.60 mm to the right during the first half of stance phase (36% of stride; 50±9% of stance), and finally moved towards the left for the remainder of the stride (Fig. 3). Ag2 had a lower mean roll value than the other alligators (Fig. 3E).

SCJ movements

SCJ protraction/retraction, abduction/adduction, pronation/supination and translation along the long axis of the joint produced patterned curves that exceeded noise thresholds set by the validation test (Fig. 4, Table 3). Medio-lateral and vertical translation curves showed patterns matching stride timing, but magnitudes were below the noise threshold (mean ranges of 0.4±0.5 mm and 1.4±0.9 mm, respectively) (Table 3).

Mean SCJ stride protraction/retraction range was 10.1±3.5 deg, with maximum protraction (6.3±4.3 deg) reached at 27% of stride (38±17% of stance). SCJ retraction followed during the latter part of stance, reaching a peak of −3.3±2.4 deg at 64% stride (88±6% of stance) (Fig. 4, blue). Ag2 differed from the other three alligators in SCJ protraction/retraction range, peak protraction and peak retraction (Fig. 3E, Table 3; one-way ANOVA $P<0.05$). For the three non-differing alligators, mean SCJ protraction/retraction range was 11.3±3.1 deg, peak protraction was 8.4±2.1 deg and peak retraction was −3.3±2.4 deg. For Ag2, mean SCJ protraction/retraction range was 6.2±0.6 deg, peak protraction was −0.3±0.8 deg and peak retraction was −5.9±0.7 deg.

Mean SCJ stride abduction/adduction range was 9.1±3.0 deg (Fig. 4B, green rotation), but Ag4 (mean range 5.8±0.8 deg) differed significantly from the other three alligators (10.21±2.5 deg; $P<0.05$). The general shape of the abduction/adduction curves was similar, with increasing abduction during stance and increasing adduction during swing, but the offset between curves generated a high standard deviation when results from all individuals were combined (Fig. 4B,E). The means for Ag2 and Ag4 were well above and well below those for the other alligators, respectively.

Mean SCJ stride pronation/supination range was 25.4±5.9 deg (Fig. 4, red). At the beginning of stance, the SCJ supinated such that the scapulocoracoid angle in lateral view became steeper (Fig. 4C). Peak supination (−13.8±2.6 deg) was reached during early stance (11±7% of stride; 16% of stance), and peak pronation (11.2±5.7 deg) near the end of stance (59±5% of stride; 81% of stance). Ag2 differed significantly from other individuals in pronation/supination range and peak pronation (Fig. 4E, Table 3). For the

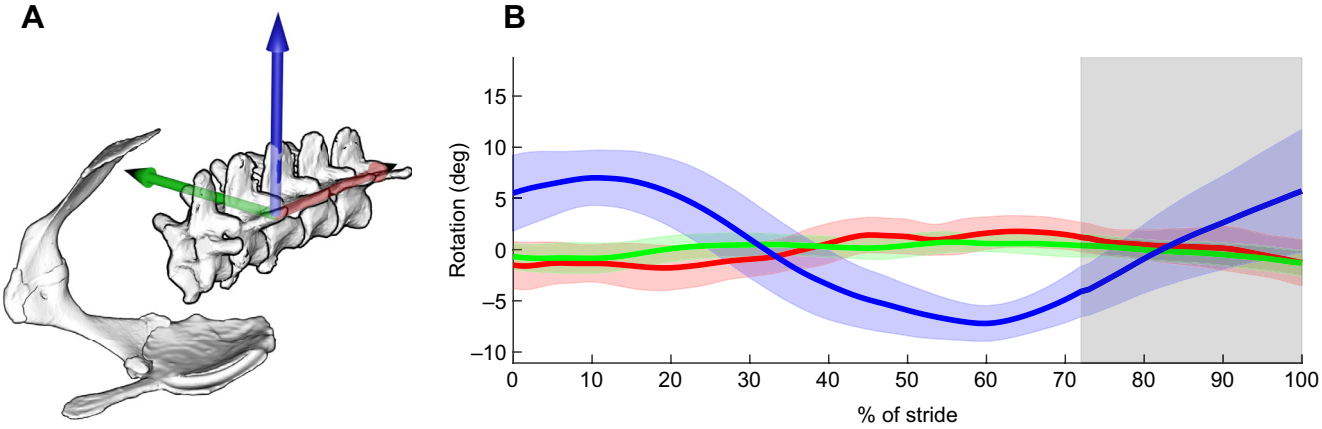

Fig. 2. Vertebral kinematics. (A) Dorsal/medial/cranial view of the anatomical coordinate system of the thoracic vertebral segments. (B) Rotations about the yaw (blue), pitch (green) and roll (red) axes during the mean stride (solid line) calculated from data from all individuals (n=36). Shaded boundaries represent ±1 s.d. White area indicates stance; gray area indicates swing.

Journal of Experimental Biology (2018) 221, jeb186791. doi:10.1242/jeb.186791

Table 3. Axial kinematics

	All (*N*=36)	Ag1 (*N*=9)	Ag2 (*N*=9)	Ag3 (*N*=9)	Ag4 (*N*=9)
Vertebral motion					
Height mean (mm)	93.4±14.9	93.8±2.5	112.6±5.5	85.5±11.3	81.7±6.5
Height range (mm)	15.4±6.2	12.0±1.8	15.9±3.4	17.4±10.7	16.2±4.9
Yaw range mean (deg)	18.4±4.5	17.2±1.2	17.1±1.8	20.9±8.1	18.4±2.8
Pitch range mean (deg)	4.2±1.3	3.5±0.7	3.5±0.6	5.0±1.5	5.0±1.3
Roll range (deg)	7.6±2.7	7.2±1.3	7.3±1.3	9.4±4.5	6.7±2.1
Sternum					
Yaw range (deg)	25.8±6.0	24.8±1.0	23.8±1.3	22.6±3.1	32.2±9.0
Pitch range (deg)	5.8±1.9	4.3±2.0	6.1±1.0	7.1±2.4	5.6±0.8
Pitch mean (deg)	17.6±3.6	21.5±2.1	16.2±1.5	13.3±1.4	19.6±2.1
Roll range (deg)	23.5±5.2	28.1±1.5	26.1±3.1	22.3±3.6	17.6±4.6
Translation *Y* (cm)	11.9±6.0	7.7±1.4	8.4±2.0	21.5±2.5	9.8±1.8
Sternocoracoid joint					
Translation *Y* (mm)	8.6±1.0	8.6±0.4	8.5±0.6	9.5±1.3	7.8±0.7
Translation *Y* (% joint length)	45.0±5.2	43.0±2.0	42.5±3.0	54.6±7.5	40.7±3.7
Protraction/retraction range (deg)	10.1±3.5	11.6±1.8	6.2±0.6	12.2±3.3	10.2±3.8
Protraction max. (deg)	6.7±4.2	9.1±1.4	0.3±0.9	9.8±2.9	7.6±1.3
Retraction min. (deg)	−3.4±2.3	−2.5±0.6	−5.9±0.7	−2.4±1.5	−2.6±3.3
Abduction range (deg)	9.1±3.0	11.1±1.9	9.0±1.6	10.6±3.5	5.8±0.8
Abduction max. (deg)	2.2±9.3	2.1±1.4	15.2±1.2	1.1±4.5	−9.8±1.3
Abduction min. (deg)	−6.9±8.3	−9.0±1.3	6.2±2.0	−9.4±2.6	−15.5±1.2
Pronation range (deg)	25.4±5.9	27.7±1.8	19.4±2.8	27.3±4.5	27.1±8.0
Supination max. (deg)	11.2±5.7	12.5±1.6	4.8±2.2	14.7±4.2	12.8±7.1
Pronation min. (deg)	−14.2±2.1	−15.2±1.5	−14.6±1.3	−12.6±2.6	−14.3±2.2
Glenohumeral joint					
Protraction range (deg)	60.5±11.9	58.6±2.3	46.4±6.7	70.6±11.4	66.3±7.4
Protraction max. (deg)	4.3±9.9	0.6±1.6	−6.1±5.9	9.9±10.1	12.7±5.9
Retraction min. (deg)	−56.2±4.8	−57.9±1.5	−52.5±2.4	−60.7±5.1	−53.6±3.9
Abduction range (deg)	39.5±5.9	34.2±4.3	42.3±4.2	42.4±7.1	39.3±4.2
Abduction max. (deg)	16.1±5.8	10.3±3.0	19.7±3.5	15.0±6.5	19.4±4.1
Abduction min. (deg)	−23.4±4.9	−23.9±2.8	−22.6±2.8	−27.4±7.1	−19.9±2.6
Pronation/supination range (deg)	38.8±7.9	38.8±1.8	28.3±2.5	47.5±5.9	40.6±4.3
Supination max. (deg)	−2.0±6.4	2.6±1.5	−9.1±2.5	2.9±5.6	−4.3±4.9
Pronation min. (deg)	−40.7±5.4	−36.1±1.1	−37.4±2.0	−44.6±6.4	−44.9±3.1

Data are means±s.d.

three non-differing alligators, pronation/supination range was 27.4±5.2 deg and peak pronation was 13.3±4.8 deg. For Ag2, pronation/supination range was 19.4±2.8 deg and peak pronation was 4.8±2.2 deg.

The coracoid translated 8.6±1.0 mm, or 45.0±5.2% of the length of the sternal groove (Fig. 4B, green translation). At the beginning of stance, the coracoid was sliding cranially, reaching its peak cranial translation of 0.5±2.3 mm at 11±8% of stride (16% of stance). The coracoid then slid caudally, reaching its peak caudal translation (7.8±3.2 mm) at 57% of stride (79±8% of stance).

GHJ movements

Mean GHJ stride protraction/retraction (Fig. 5, blue) range was 60.5±11.9 deg, with peak stance protraction (−5.5±10.3 deg) occurring at 1% of stride (2±1% of stance). The GHJ retracted during stance, reaching peak retraction of −55.4±4.9 deg at 67% of stride (93±12% of stance). Ag2 differed significantly (Table 3) in mean protraction/retraction range (46.4±6.7 deg) from the other three alligators (65.2±9.2 deg).

Mean GHJ stride abduction/adduction range (Fig. 5, green) was 39.5±5 deg, and maximum abduction (−21.5±6.4 deg) was reached at 15% of stride (21±16% of stance). The GHJ adducted through mid-swing, reaching a peak of 16.1±5.8 deg at 80% of stride (29±4% of swing).

Mean GHJ stride pronation/supination range (Fig. 5, red) was 38.8±7.9 deg. The GHJ was pronating at the beginning of stance and continued to pronate to a peak of −2.5±6.4 deg at 45% of stride (63±11% of stance). The GHJ supinated through late swing, reaching peak supination (−39.7±6.2 deg) at 95±5% of stride (80±5% of swing).

Stride length effects

We measured the contribution of each joint to stride length using three different methods: (1) sequentially removing joint movements from distal to proximal, (2) sequentially removing joint movements from proximal to distal, and (3) removing each joint movement individually (Table 4). Joint motion was removed by freezing each degree of freedom at its mean value throughout the stride being analyzed. Its effect on stride length was measured as the percentage change in stride length. All nine strides were used for all alligators except Ag3, in which the wrist was visible in only six strides.

For all three methods, all joints were found to contribute positively to stride length (removal of joint motion caused a reduction in stride length). When removing joints individually, vertebral motion reduced stride length by 6.2±3.7%, sternum by 10.7±4.5%, SCJ by 9.3±4.6%, GHJ by 38.0±6.5% and elbow by 21.4±3.9% (Table 4).

Removing joints sequentially from distal to proximal made the largest difference in stride length estimates, particularly vertebral motion (14.5±4.8%) and sternum (17.4±5.6%), a difference of +8.3% and +6.7%, respectively, when compared with removing individual joints. The results for the remaining joints were more comparable to individual removal of joints: SCJ 10.6±4.8%, GHJ 36.1±4.5% and elbow 21.4±3.9%. Sequential removal from proximal to distal resulted in a larger estimated elbow contribution of 31.1±4.2%, a difference of 9.7%, but results from the remaining joints were more comparable those obtained from

Journal of Experimental Biology (2018) 221, jeb186791. doi:10.1242/jeb.186791

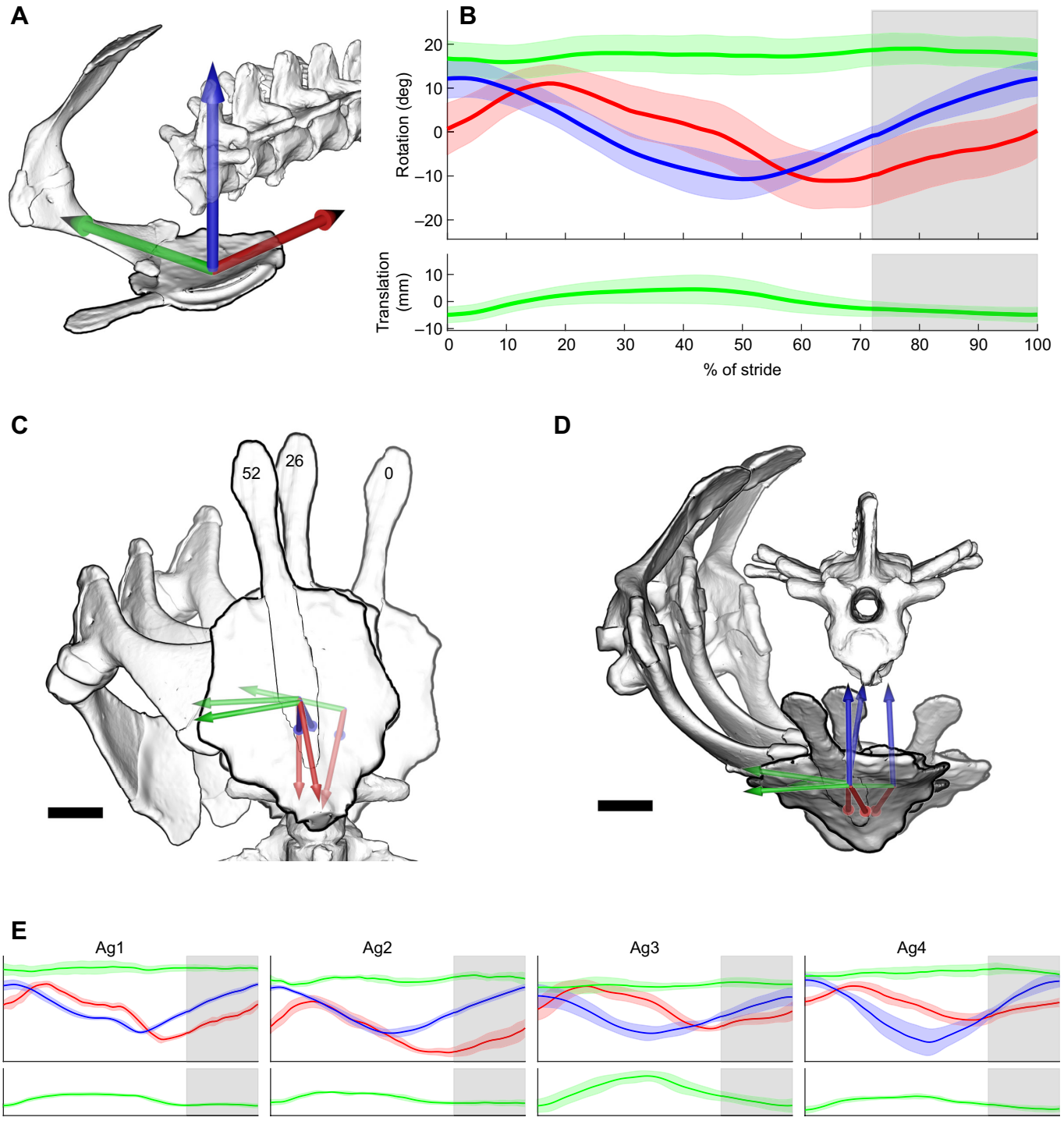

Fig. 3. Sternal kinematics. (A) Dorsal/medial/cranial view of the sternum and right shoulder girdle with sternal axes in the zero position relative to the vertebral column. (B) Rotations (top) about the yaw (blue), pitch (green) and roll (red) axes and translation (bottom) along the lateral axis (green) during the mean stride (solid line) for all individuals (n=36). Shaded boundaries represent ±1 s.d. (C) Ventral view of the sternal movements relative to the vertebral column from the beginning of stance (0% stride) to peak yaw (52% of stride; 72% of stance). (D) Cranial view from the beginning of stance to peak yaw. Scale bars: 10 mm. (E) Mean (solid line) sternal kinematics for individual alligators (n=9 each). Shaded boundaries represent ±1 s.d. White area on graphs indicates stance; gray area indicates swing.

removing joints individually: vertebral motion 7.6±3.6%, sternum 11.1±2.5%, SCJ 10.1±5.2% and GHJ 40.1±7.8%.

Rigidity of the elements

We addressed three questions regarding whether or not individual elements behave as expected for rigid bodies. (1) Do the marked 3–4 thoracic vertebrae move as a single rigid object? (2) Does the cartilaginous sternum deform during walking? (3) Do the scapula and coracoid act as rigid elements?

IMD variation between markers on the same rigid element should be very low, representing only the accumulated errors of the XROMM process. For all markers, there was a clear distinction between markers on the same skeletal segment and those on different elements. However, not all markers on the

Journal of Experimental Biology (2018) 221, jeb186791. doi:10.1242/jeb.186791

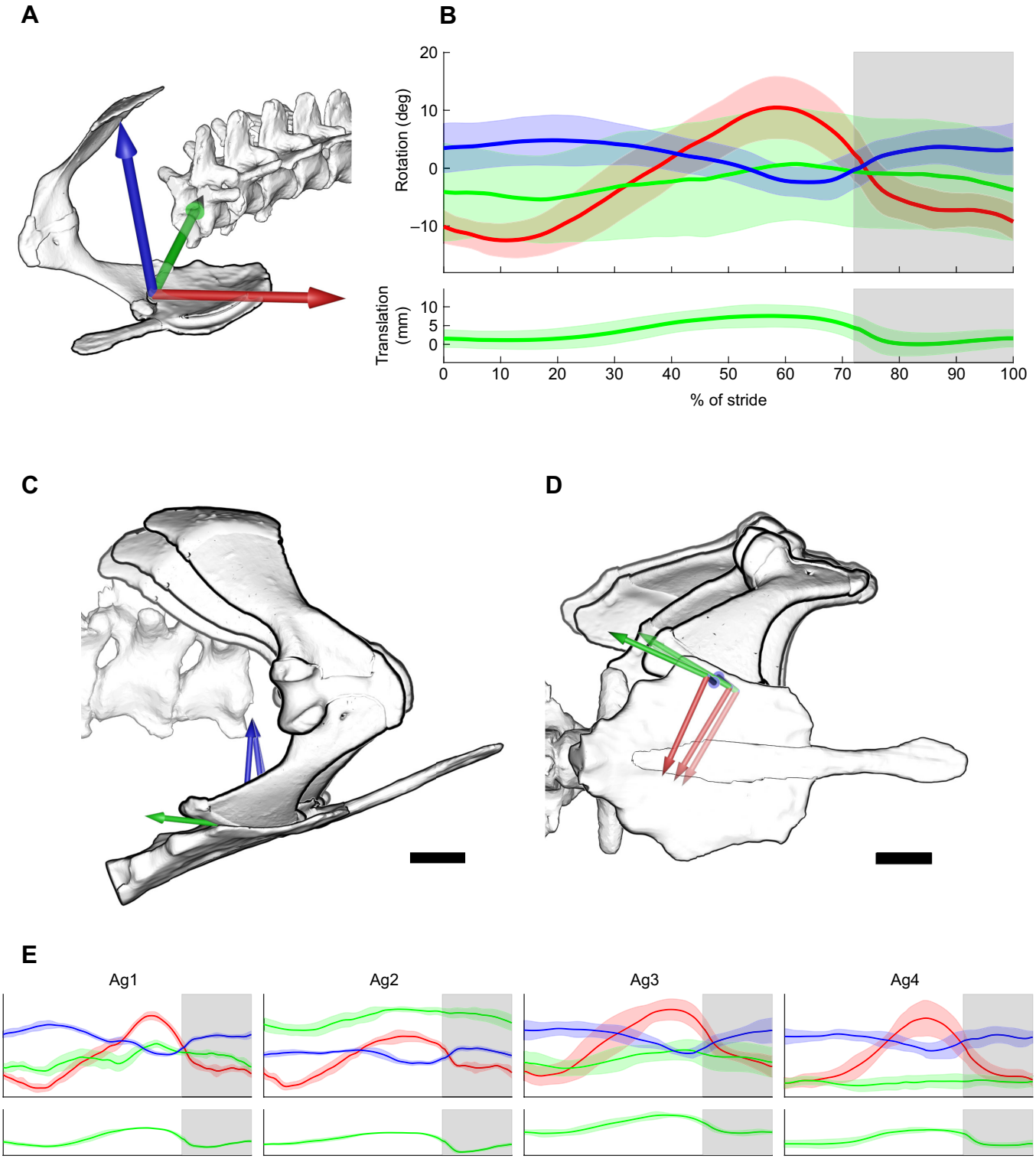

Fig. 4. Sternocoracoid kinematics. (A) Dorsal/medial/cranial view of the sternum and right shoulder girdle with sternocoracoid joint (SCJ) axes in the zero position relative to the sternum. (B) Rotations (top) about the yaw (blue), abduction/adduction (green) and roll (red) axes and translation (bottom) along the sternal groove axis (green) during the mean stride (solid line) for all individuals (n=36). Shaded boundaries represent ±1 s.d. (C) Lateral view of the SCJ movements relative to the sternum from the beginning of stance (0% stride) to peak SCJ translation (green; 59% of stride; 82% of stance). (D) Ventral view from the beginning of stance to peak yaw. For C and D, the lightest outline outline is at 0% of stride, the middle shade outline is 30% of stride and the darkest outline is 60% of stride. Scale bars: 10 mm. (E) Mean (solid line) SCJ kinematics for individual alligators (n=9 each). Shaded boundaries represent ±1 s.d. White area on graphs indicates stance; gray area indicates swing.

same element were below the threshold established for truly rigid elements. The first and last markers on the vertebral column tended to have higher residuals than markers close to each other, as would be expected if very small intervertebral movements accumulated across the span of five vertebrae. In Ag1, the difference between the caudal-most marker and the other four

Journal of Experimental Biology (2018) 221, jeb186791. doi:10.1242/jeb.186791

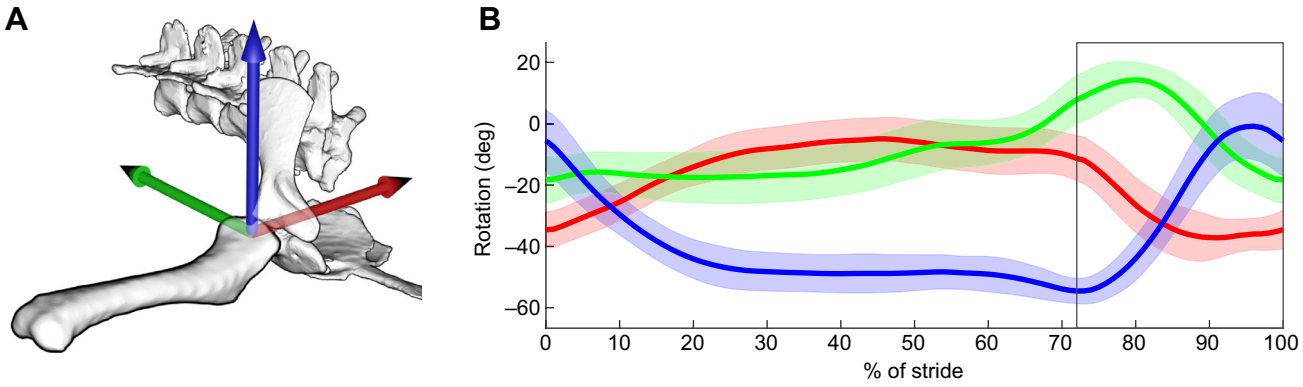

Fig. 5. Glenohumeral kinematics. (A) Antero-lateral view of the joint coordinate system of the glenohumeral joint in its reference pose. (B) Rotations about the yaw (blue), pitch (green) and roll (red) axes during the mean stride for all individuals (*n*=36).

markers was an order of magnitude larger than IMD standard deviation between any of the other four markers and was thus discarded in rigid body calculations.

Three of the specimens had at least three markers on the sternum or interclavicle with residuals within the predicted range for rigid bodies. In two cases, a marker was placed in the caudal xiphisternal process, yielded much higher residuals than the others, and was excluded from rigid body calculations. Ag2 had only three usable sternal markers and one of them was placed very close to the groove of the SCJ. This marker had residuals in the 'gray area' close to the maximum residuals expected for a marker on the same rigid body as the other two, and likely affected the rigid body calculations. All markers on the scapula and coracoid had IMD residuals either below or very close to the estimated threshold for rigid bodies.

DISCUSSION

In this study, we found that both sternal rotation and sternocoracoid sliding contribute to displacement of the scapulocoracoid during alligator high walks. To our knowledge, this is the first evidence of sternal rotation relative to the vertebral column contributing to stride length in any tetrapod. A previous study reported that alligator scapulocoracoid movement contributed ca. 30% to stride length during alligator high walks, but this estimate assumed that the sternocoracoid joint was the only source of mobility within the pectoral skeleton (Baier and Gatesy, 2013). In this study, total scapulocoracoid contribution to stride length was comparable (28%) when measured similarly. [Baier and Gatesy (2013) measured stride contribution by first fixing the vertebral translations (inertial reference frame) and then subtracting joint effects by fixing joints distal to proximal. Here, we adopt the more conservative measurements resulting from proximal-to-distal as described later in this section.] However, measurements of individual elements show that sternum movement contributed 17% to stride length, while the SCJ only contributed 11%. Thus, the sternum increased stride length by rotating relative to the thoracic vertebrae, presumably via rib joints and/or bending within flexible ribs. The SCJ contributes less than originally thought but still yields an increase in stride length.

Table 4. Percentage change in stride length after removing joint movement

	All	Ag1 (*N*=9)	Ag2 (*N*=9)	Ag3 (*N*=9)	Ag4 (*N*=6)	Baier and Gatesy, 2013
Vertebral motion						
Distal to proximal (%)	14.5±4.8	9.3±1.0	17.8±3.9	16.2±6.1	15.2±2.8	16.7±3.0
Proximal to distal (%)	6.2±3.7	5.7±1.6	9.8±2.6	4.2±4.5	4.6±3.6	–
Individual (%)	6.2±3.7	5.7±1.6	9.8±2.6	4.2±4.5	4.6±3.6	–
Sternum						
Distal to proximal (%)	17.4±5.6	14.7±1.7	23.4±1.7	13.1±4.2	17.0±6.8	–
Proximal to distal (%)	11.1±2.5	10.3±1.8	12.4±1.7	8.4±2.9	12.4±1.7	–
Individual (%)	10.7±4.5	8.8±1.6	11.9±1.6	6.4±3.1	14.2±6.2	–
SCJ						
Distal to proximal (%)	10.6±4.8	12.7±2.1	7.4±1.2	12.7±9.3	10.2±3.8	–
Proximal to distal (%)	10.1±5.2	8.3±1.1	8.8±1.0	16.5±10.4	8.8±1.0	–
Individual (%)	9.3±4.6	8.3±1.2	8.7±1.2	14.1±8.8	7.6±3.3	–
Sternum+SCJ						
Distal to proximal (%)	28.0±5.2	27.4±3.7	30.8±2.8	25.8±13.5	27.2±10.6	30.5±3.0
Proximal to distal (%)	21.2±3.9	18.6±1.5	21.1±1.4	24.9±6.7	21.1±1.4	–
Individual (%)	20.0±5.5	17.1±1.4	20.6±2.7	20.6±8.1	21.8±5.0	–
GHJ						
Distal to proximal (%)	36.1±4.5	38.8±1.7	32.7±3.8	35.0±5.6	37.7±4.5	24.2±5.0
Proximal to distal (%)	40.1±7.8	47.2±2.2	36.3±7.1	41.1±8.9	36.3±7.1	–
Individual (%)	38.0±6.5	42.8±1.7	32.1±4.2	37.3±7.4	39.7±6.7	–
Elbow						
Distal to proximal (%)	21.4±3.9	24.4±1.3	18.7±2.1	22.9±6.8	19.9±2.2	19±6.0
Proximal to distal (%)	31.1±4.2	28.5±0.9	32.8±4.3	29.8±5.4	32.8±4.3	–
Individual (%)	21.4±3.9	24.4±1.3	18.7±2.1	22.9±6.8	19.9±2.2	–

SCJ, sternocoracoid joint; GHJ, glenohumeral joint. Data are means±s.d.

Baier and Gatesy (2013) measured individual joint contributions by first removing the translations of the whole body and then sequentially 'freezing' joints from distal to proximal (DP) and re-measuring stride length. However, other studies have removed joint effects from proximal to distal (PD) (Fischer and Lehmann, 1998). Both approaches were employed in this study, as was the additional method of removing joints individually. Removing joints individually provides a general sense of how much each joint is contributing to stride length but the sum of the individual joint contributions will never equal 100% because the timing of stance and swing does not perfectly match the turnaround timing of any one joint.

DP joint removal assigns greater stride contributions to the proximal joints. PD joint removal assigns greater contributions to distal joints but matches removal of individual joints more closely (Table 4). All methods agree closely for the SCJ (11% PD, 10% DP, 9% individual; Table 4). However, the DP approach may over-estimate the contributions from sternal motion (17% DP, 11% PD, 11% individual; Table 4) and vertebral lateral bending (15% PD, 6% DP, 6% individual; Table 4).

We view adoption of PD joint removal as more appropriate for this study as it yields more conservative stride length contribution estimates for movements of the axial skeleton and does not over-inflate the importance of the vertebral and sternal contributions. Additionally, PD is more widely used (Fischer et al., 2010; Nyakatura and Fischer, 2010) and thus allows easier comparison with other studies. Thus PD estimates of 6% for the vertebral column, 11% for sternal motion and 10% for the sternocoracoid joint are adopted here.

Axial movements

Lateral bending of the vertebral column during locomotion is common among non-mammalian, non-avian vertebrates (Ritter, 1992), and increases stride length in tetrapods. Bending along the vertebral column has been shown to follow a standing wave pattern in alligators with the node (point of little rotation) lying slightly caudal to the level of the shoulder girdle (Reilly and Elias, 1998), and approximately corresponding to the more cranial thoracic segments marked in this study. We found little intervertebral movement in this region, suggesting that lateral bending of the caudal thoracic and lumbar regions yaws the relatively stiff thoracic/pectoral region. This movement, in turn, displaces the sternum and scapulocoracoid, increasing the excursion of the pectoral limb. Molnar et al. (2014) found lower stiffness in more cranial thoracic joints compared with more caudal vertebral joints in vertebral columns that had been removed by dissection. The discrepancy between their *ex vivo* results and our *in vivo* results may be explained by the stiffening effects of the rib cage and shoulder girdle, and by the mechanical loading pattern on the vertebral column.

Vertebral bending has been linked to a trade-off between breathing and locomotion (Carrier, 1987a,b; Owerkowicz et al., 1999), in that conflicting demands on axial muscles limit breathing capacity during running in lizards. A similar conflict exists in alligators, but may be mitigated by the reduced amount of lateral bending associated with the more upright posture, and also by compensation via the diaphragmaticus mechanism (Farmer and Carrier, 2000). Here, we found that the thoracic region of the vertebral column is relatively stiff, but the observed rotation of the sternum relative to the thoracic vertebrae indicates that the ribcage must be changing shape. The source of the movement must be the rib joints and/or flexible ribs, rather than intervertebral movements. Bending of the spine cranial and caudal to the stiff thoracic region would passively cause some ribcage deformation, and the rotation of the sternum relative to the thoracic vertebrae would compound this effect. The cause of sternal movements relative to the spine, whether active or passive, warrants further investigation. Additionally, it would be interesting to know how widespread this phenomenon is among terrestrial vertebrates.

Combined sternal yaw and lateral translation yields a 2D center of rotation in the dorsoventral plane that approximately corresponds to the bending zone between the prosternum and mesosternum (Fig. 1B). This suggests that the prosternum can rotate relative to the vertebral column via movements of ribs 1 and 2 while the mesosternum maintains a fixed orientation with respect to the caudal thorax and abdomen. However, given that the mesosternum is narrow and flexible, we hypothesize a gradual change of orientation between the first two ribs and more caudal ones.

Small, juvenile alligators were used in this study. Although the sternum remains cartilaginous in fully grown alligators (Gegenbaur, 1876), some reduction in flexibility may occur with increasing age. Data on the material properties and mobility of the sternum in larger alligators would help to clarify this issue.

SCJ movements

SCJ contribution to stride length was smaller than originally measured (Baier and Gatesy, 2013), but did contribute positively to stride length (ca. 11%). Although sliding of the tongue and groove joint was substantial (the coracoid tongue translating 45% of the length of the sternal groove), the muscles anchoring the scapula to the thorax appear to constrain the movement of the scapulocoracoid as a whole, thus limiting the overall displacement of the glenoid.

The scapula and coracoid move as a single rigid body. There is no evidence of movement between the scapula and coracoid during locomotion. However, if one aligns the coracoid model from a CT scan of an intact animal and a coracoid model of the same animal after removal of the scapulocoracoid by dissection, the scapulae do not align perfectly (D.B.B., personal observation). The scapula is deflected laterally in the scan of the isolated bones. This indicates that the scapula is under a constant medial torque *in situ*, perhaps exerted by soft tissue anchoring the dorsal scapular cartilage or the overlying skin.

Gray (1968) suggested that non-mammalian tetrapods may employ sternocoracoid mobility to increase stride length, and sternocoracoid sliding was described in a cineradiographic study of varanid lizards (Jenkins and Goslow, 1983). However, it has also been suggested that relatively fixed sternocoracoid articulations are typical in terrestrial lizards (Peterson, 1972, 1984) and that a mobile articulation is a unique modification in chameleons, which contend with arboreal constraints (Fischer et al., 2010; Peterson, 1984). A narrow branch substrate limits lateral undulations of the vertebral column, and a highly mobile coracosternal joint compensates by increasing forelimb excursion (Fischer et al., 2010).

In this study, the contribution of the SCJ was found to be comparable to that seen in chameleons (11% alligator, 8% chameleon). Crocodilians share an evolutionary loss of the clavicle with chameleons, which may be associated with the increased sternocoracoid mobility seen in both groups. However, crocodilians use their forelimbs in terrestrial locomotion, demonstrating that sternocoracoid mobility can be retained in terrestrial locomotors. It is possible that the majority of lizards follow the pattern described in Peterson (1984) for *Dipsosaurus* and *Agama*, and that the mobility found in *Varanus* is unusual. Manipulations of a single, dead *Iguana* forelimb revealed no sternocoracoid mobility (D.B.B. and S.M., personal observation),

but it should be noted that data on sternocoracoid mobility within lepidosaurs is limited and that the plesiomorphic degree of girdle mobility is unknown.

If sternocoracoid mobility is a derived state, it would appear to occur within groups with unusual constraints, such as chameleons (previously described), or turtles (Schmidt et al., 2016), in which the shell imposes limitations. Why would sternocoracoid mobility appear in crocodilians? Basal archosaurs are thought to have maintained more mammalian-like parasagittal postures (Parrish, 1987), which may have limited lateral bending. A mobile SCJ would have permitted greater limb excursion under this constraint. Loss of the clavicle could then further enhance sternocoracoid mobility in Crocodylomorpha, and this increased mobility was evidently retained despite the secondary return to intermediate postures. Further investigation is needed to understand the underlying mechanisms driving the evolution of sternal and shoulder girdle movements and the linkage between shoulder girdle morphology and clavicular loss.

Acknowledgements
We thank Beth Brainerd for sharing data from the Alligator Breathing study and for sharing alligators, and Tom Roberts for providing the surgery room and supplies. Thanks to the morphology group at Brown University for their support with the surgeries and data collection, especially Erika Tavares, Terry Dial, Nicolai Konow, Henry Astley, Angela Horner, Ariel Camp, Nick Gidmark and Rachel Menegaz; Brown University Animal Care facility for assisting with animal husbandry and surgery; and Ruth Elsey for providing dissection specimens. We greatly appreciate the efforts of the reviewers to improve and clarify the manuscript text.

Competing interests
The authors declare no competing or financial interests.

Author contributions
Conceptualization: D.B.B., B.M.G., S.M., R.M.C.; Methodology: D.B.B., B.M.G., S.M., R.M.C.; Software: D.B.B., B.M.G., S.M., R.M.C.; Validation: D.B.B., B.M.G., S.M., R.M.C.; Formal analysis: D.B.B., B.M.G., S.M., R.M.C.; Investigation: D.B.B., B.M.G., S.M., R.M.C.; Resources: D.B.B., S.M., R.M.C.; Data curation: D.B.B.; Writing - original draft: D.B.B., B.M.G.; Writing - review & editing: D.B.B., B.M.G., S.M., R.M.C.; Visualization: D.B.B., B.M.G.; Supervision: D.B.B., S.M.; Project administration: D.B.B., S.M.; Funding acquisition: D.B.B., R.M.C.

Funding
This material is based upon work supported by the National Science Foundation: [1262124, 1004057], the National Science Foundation Graduate Research Fellowship [under grant no. 75094], and a Providence College Committee to Aid Faculty Research Grant.

Data availability
Data have been deposited in the X-ray Motion Analysis Portal (xmaportal.org) in the Alligator Forelimb project (portal ID: Brown16). Raw data were also analyzed from the Alligator Lung Ventilation project (portal ID: Brown10).

References
Allen, V., Molnar, J., Parker, W., Pollard, A., Nolan, G. and Hutchinson, J. R. (2014). Comparative architectural properties of limb muscles in Crocodylidae and Alligatoridae and their relevance to divergent use of asymmetrical gaits in extant Crocodylia. *J. Anat.* **225**, 569-582.

Baier, D. B. and Gatesy, S. M. (2013). Three-dimensional skeletal kinematics of the shoulder girdle and forelimb in walking alligator. *J. Anat.* **223**, 462-473.

Brainerd, E. L., Baier, D. B., Gatesy, S. M., Hedrick, T. L., Metzger, K. A., Gilbert, S. L. and Crisco, J. J. (2010). X-ray reconstruction of moving morphology (XROMM): precision, accuracy and applications in comparative biomechanics research. *J. Exp. Zool. A Ecol. Genet. Physiol.* **313A**, 262-279.

Brainerd, E. L., Moritz, S. and Ritter, D. A. (2016). XROMM analysis of rib kinematics during lung ventilation in the green iguana, *Iguana iguana*. *J. Exp. Biol.* **219**, 404-411.

Brocklehurst, R. J., Moritz, S., Codd, J., Sellers, W. I. and Brainerd, E. L. (2017). Rib kinematics during lung ventilation in the American alligator (*Alligator mississippiensis*): an XROMM analysis. *J. Exp. Biol.* **220**, 3181-3190.

Carrier, D. R. (1987a). The evolution of locomotor stamina in tetrapods: circumventing a mechanical constraint. *Paleobiology* **13**, 326-341.

Carrier, D. R. (1987b). Lung ventilation during walking and running in four species of lizard. *Exp. Biol.* **47**, 33-42.

Chamero, B., Buscalioni, Á. D. and Marugán-Lobón, J. (2013). Pectoral girdle and forelimb variation in extant Crocodylia: the coracoid-humerus pair as an evolutionary module. *Biol. J. Linn. Soc.* **108**, 600-618.

Crisco, J. J. and McGovern, R. D. (1998). Efficient calculation of mass moments of inertia for segmented homogenous three-dimensional objects. *J. Biomech.* **31**, 97-101.

Eaton, T. H. (1944). Modifications of the shoulder girdle related to reach and stride in mammals. *J. Morphol.* **75**, 167-171.

Farmer, C. G. and Carrier, D. R. (2000). Ventilation and gas exchange during treadmill locomotion in the american alligator (*Alligator mississippiensis*). *J. Exp. Biol.* **203**, 1671-1678.

Fischer, M. S. and Lehmann, R. (1998). Application of cineradiography for the metric and kinematic study of in-phase gaits during locomotion of the pika (Ochotona rufescens, Mammalia: Lagomorpha). *Zoology* **101**, 148-173.

Fischer, M. S., Krause, C. and Lilje, K. E. (2010). Evolution of chameleon locomotion, or how to become arboreal as a reptile. *Zoology* **113**, 67-74.

Gatesy, S. M. (1991). Hind limb movements of the American alligator (*Alligator mississippiensis*) and postural grades. *J. Zool.* **1991**, 577-588.

Gegenbaur, C. (1876). Einige Bemerkungen zu Götte's, Entwickelungsgeschichte der Unke als Grundlage einer vergleichenden Morphologie der Wirbelthiere. *Morphol. Jahrb.* **1**, 299-345.

Gray, S. J. (1968). *Animal Locomotion*. London: Weidenfeld and Nicolson.

Hutchinson, J. R. (2006). The evolution of locomotion in archosaurs. *Comptes Rendus Palevol.* **5**, 519-530.

Hutson, J. D. and Hutson, K. N. (2012). A test of the validity of range of motion studies of fossil archosaur elbow mobility using repeated-measures analysis and the extant phylogenetic bracket. *J. Exp. Biol.* **215**, 2030-2038.

Hutson, J. D. and Hutson, K. N. (2013). Using the American alligator and a repeated-measures design to place constraints on in vivo shoulder joint range of motion in dinosaurs and other fossil archosaurs. *J. Exp. Biol.* **216**, 275-284.

Hutson, J. D. and Hutson, K. N. (2014). A repeated-measures analysis of the effects of soft tissues on wrist range of motion in the extant phylogenetic bracket of dinosaurs: implications for the functional origins of an automatic wrist folding mechanism in crocodilia. *Anat. Rec.* **297**, 1228-1249.

Iijima, M., Kubo, T. and Kobayashi, Y. (2018). Comparative limb proportions reveal differential locomotor morphofunctions of alligatoroids and crocodyloids. *R. Soc. Open Sci.* **5**.

Jenkins, F. A. and Goslow, G. E. J. (1983). The functional anatomy of the shoulder of the Savannah monitor lizard (*Varanus exanthematicus*). *J. Morphol.* **175**, 195-216.

Kälin, J. (1929). Uber den Brustschulterapparat der Krokodile. *Acta Zool.* **10**, 343-399.

Knorlein, B. J., Baier, D. B., Gatesy, S. M., Laurence-Chasen, J. D. and Brainerd, E. L. (2016). Validation of XMALab software for marker-based XROMM. *J. Exp. Biol.* **219**, 3701-3711.

Maidment, S. C. R., Bates, K. T., Falkingham, P. L., VanBuren, C., Arbour, V. and Barrett, P. M. (2014). Locomotion in ornithischian dinosaurs: an assessment using three-dimensional computational modelling. *Biol. Rev.* **89**, 588-617.

Meers, M. B. (2003). Crocodylian forelimb musculature and its relevance to archosauria. *Anat. Rec. A Discov. Mol. Cell. Evol. Biol.* **274A**, 891-916.

Menegaz, R. A., Baier, D. B., Metzger, K. A., Herring, S. W. and Brainerd, E. L. (2015). XROMM analysis of tooth occlusion and temporomandibular joint kinematics during feeding in juvenile miniature pigs. *J. Exp. Biol.* **218**, 2573-2584.

Molnar, J. L., Pierce, S. E. and Hutchinson, J. R. (2014). An experimental and morphometric test of the relationship between vertebral morphology and joint stiffness in Nile crocodiles (Crocodylus niloticus). *J. Exp. Biol.* **217**, 758-768.

Nyakatura, J. A. and Fischer, M. S. (2010). Three-dimensional kinematic analysis of the pectoral girdle during upside-down locomotion of two-toed sloths (*Choloepus didactylus*, Linné 1758). *Front. Zool.* **7**, 1-21.

Otero, A., Allen, V., Pol, D. and Hutchinson, J. R. (2017). Forelimb muscle and joint actions in Archosauria: insights from Crocodylus johnstoni (Pseudosuchia) and Mussaurus patagonicus (Sauropodomorpha). *PeerJ* **5**, e3976.

Owerkowicz, T., Farmer, C. G., Hicks, J. W. and Brainerd, E. L. (1999). Contribution of gular pumping to lung ventilation in monitor lizards. *Science* **284**, 1661-1663.

Padian, K. (2008). Were pterosaur ancestors bipedal or quadrupedal?: morphometric, functional, and phylogenetic considerations. *Zitteliana Reihe B. Abhandlungen der Bayerischen Staatssammlung für Paläontologie und Geologie* **28**, 21.

Padian, K., Li, C. and Pchelnikova, J. (2010). The trackmaker of Apatopus (late triassic, North America): implications for the evolution of archosaur stance and gait. *Palaeontology* **53**, 175-189.

Parrish, J. M. (1987). The origin of crocodilian locomotion. *Paleobiology* **13**, 396-414.

Persons, W. S. and Currie, P. J. (2017). The functional origin of dinosaur bipedalism: cumulative evidence from bipedally inclined reptiles and disinclined mammals. *J. Theor. Biol.* **420**, 1-7.

Peterson, J. (1972). Lateral undulation and biomechanics of shoulder girdle. *Am. Zool.* **12**, 729.
Peterson, J. A. (1984). The locomotion of *Chamaeleo* (Reptilia: Sauria) with particular reference to the forelimb. *J. Zool.* **202**, 1-42.
Reilly, S. M. and Elias, J. A. (1998). Locomotion in Alligator mississippiensis: kinematic effects of speed and posture and their relevance to the sprawling-to-erect paradigm. *J. Exp. Biol.* **201**, 2559-2574.
Ritter, D. (1992). Lateral bending during lizard locomotion. *J. Exp. Biol.* **173**, 1-10.
Schmidt, M., Mehlhorn, M. and Fischer, M. S. (2016). Shoulder girdle rotation, forelimb movement and the influence of carapace shape on locomotion in *Testudo hermanni* (Testudinidae). *J. Exp. Biol.* **219**, 2693-2703.
VanBuren, C. S. and Bonnan, M. (2013). Forearm posture and mobility in quadrupedal dinosaurs. *PLoS ONE* **8**, e74842.